JOURNAL OF THERMOPHYSICS AND HEAT TRANSFER
Vol. 6, No. 4, Oct.–Dec. 1992

Refractive Index Effects on Radiative Behavior of a Heated Absorbing-Emitting Layer

C. M. Spuckler* and R. Siegel†
NASA Lewis Research Center, Cleveland, Ohio 44135

Temperature distributions and other heat transfer characteristics are analyzed for a heated plane layer of semitransparent material with refractive index ≥1. The analysis includes heat conduction, emission, and absorption within the layer. The layer has diffuse interfaces; examples are a frosted quartz window used to diffuse incident radiation in high temperature surroundings, or a ceramic layer with small scattering used in high-temperature applications. Each side of the layer is heated by radiation and convection, and interface reflections are included. When the index of refraction is larger than unity, there are total internal reflections of some of the energy within the layer. This has a substantial effect on distributing energy across the layer, and considerably alters the temperature distribution from when the refractive index is unity. Results are given for a gray layer and for a two-band spectral variation of the absorption coefficient. Radiant energy leaving the surface was examined to determine when it could be used to measure surface temperature accurately.

Nomenclature

A = quantity defined in Eq. (12c)
a = absorption coefficient of layer, m^{-1}
C = quantity defined in Eqs. (12d) and (12e); $\bar{C} = C/\sigma T_{g1}^4$
C_2 = blackbody radiation constant, m·K
c_0 = velocity of electromagnetic propagation in vacuum, m/s
D = thickness of plane layer, m
dq_ν = spectral flux in a differential interval of frequency, W·s/m²
E_2, E_3 = exponential integral functions, $E_n(x) = \int_0^1 \mu^{n-2} \exp(-x/\mu)\, d\mu$
$e_{\nu b}$ = blackbody hemispherical spectral radiation for $n = 1$, W·s/m²
$F_{0-\nu}$ = blackbody fraction in frequency range 0 to ν
H_R = dimensionless convection-radiation parameter, $h_1/\sigma T_{g1}^3$
h = convective heat transfer coefficient, W/m²·K
k = thermal conductivity of radiating medium, W/m·K
N_D = conduction-radiation parameter based on length D, $k/\sigma T_{g1}^3 D$
n = index of refraction
q = heat flux, W/m²; $\bar{q} = q/\sigma T_{g1}^4$
q_r = radiative heat flux, W/m²
R = ratio of heat transfer coefficients, h_1/h_2
T = absolute temperature, K
T_g = gas temperature, K
T_{s1}, T_{s2} = temperatures of radiating surroundings, K
t = dimensionless temperature, T/T_{g1}
x = coordinate normal to boundary of plane layer, m; $X = x/D$
β = quantity defined in Eq. (27b)
ε = emissivity of surface for an opaque layer
κ = optical coordinate $a \cdot x$; κ_D, optical thickness, $a \cdot D$
ρ^i = reflectivity of interface for internally incident radiation
σ = Stefan-Boltzmann constant, W/m²·K⁴
τ^o = transmissivity of interface for externally incident radiation

Subscripts

a = apparent surface temperature from heat flux
g = gas on either side of layer
i, o = incoming and outgoing radiation
k = the kth frequency band
l, s = long and short wavelength regions
r = radiative quantity
ν = frequency
1, 2 = the hot and cooler surroundings of the layer

Received June 17, 1991, revision received Sept. 20, 1991; accepted for publication Sept. 21, 1991.

*Research Scientist, Heat Transfer Branch.
†Research Scientist, Lewis Research Academy. Fellow AIAA.

Introduction

THE temperature distribution in a semitransparent material can be significantly influenced by its index of refraction. If there is external radiant heating, the refractive index affects the amount of external energy reflected and transmitted from the outside into the interior of the material. A much more significant factor is that radiation emitted from within the material volume depends on the *square* of its index of refraction. As the refractive index is increased, the internal volume emission can be many times that emitted by a blackbody radiating into a vacuum. Because radiation exiting from an interface cannot exceed that of a blackbody, there is extensive energy reflection at the internal interfaces, most of it by total internal reflection. This can have a substantial effect on the layer temperature distribution.

The present analysis examines the effects of index of refraction and other independent parameters on the temperature distributions in a semitransparent plane layer. The layer is subjected to external radiative and convective heating at each of its surfaces. The material emits and absorbs radiation, but for the type of layer considered here, scattering is small except at the interfaces. The layer is a crystal or window-type of material, hence its absorption coefficient is a function of the radiation frequency. Results are provided for a gray layer and for a two-band spectral variation of the absorption coefficient. The results include temperature distributions, surface temperatures, and apparent surface temperatures an optical

pyrometer would measure based on radiant energy received. The gray results are found to provide a guide for the spectral behavior. The surfaces have been roughened deliberately, or have become roughened by erosion, or are contaminated. Hence, the surfaces act to diffuse radiation transmitted or reflected at the boundaries. Diffuse boundary conditions are used in the analysis. An application with this type of moderately roughened layer is the use of a frosted quartz window to diffuse incident radiation from an intense lamp source in a high-temperature experiment using radiant heating. The temperature level and distribution in the window must be estimated in the design of the experiment. The results are also applicable to some ceramic materials that have small scattering and are used in high-temperature applications where temperature distributions and gradients are important.

The layer reaches an equilibrium temperature distribution, depending on the surrounding heating or cooling environments that provide radiation and convection. The effects on the layer temperature distribution of the index of refraction, layer optical thickness, and thermal conductivity are investigated for various magnitudes of the external heat transfer conditions.

An analysis of temperature distributions in absorbing-emitting layers, including index of refraction effects was developed by Gardon[1] to predict cooling and heat treating of glass plates. The interfaces were optically smooth so reflections are specular and are computed from the Fresnel reflection laws. Another application, for which a computer program was developed, was for the heating of a window in a reentry vehicle.[2] A number of recent papers[3-5] have examined further the effects of Fresnel boundary reflections and nonunity refractive index. Some other examples of analysis of both steady and transient heat transfer to single or multiple plane layers[6-8] have used diffuse assumptions at the interfaces. A study in Ref. 9 includes spectral effects and directional effects at bounding solid walls. Directional variations in the emission-reflection characteristics of the solid walls were found to have small effects. The present authors have not found a detailed analysis for a layer subjected to the type of heating conditions studied here. This includes the effects of diffuse interfaces without enclosing solid boundaries, the total reflection of a portion of the internally radiated energy, and a nonunity refractive index. The analysis is given for a general spectral variation in the absorption coefficient.

Analysis

Relations for Temperature Distribution from Energy Equation

The layer geometry and coordinate system are shown in Fig. 1. The layer has thickness D, constant index of refraction n, and spectral absorption coefficient a_ν. There are specified diffuse radiative heat fluxes q_{r1} and q_{r2} incident on each of the sides. There is also convective heat transfer on each side provided by gas temperatures T_{g1} and T_{g2} and convective heat transfer coefficients h_1 and h_2. The conditions are such that side 1 is the higher temperature side.

Energy is transferred within the semitransparent material by conduction and radiation so the energy equation contains a term for each of these modes. The total energy flux transferred by radiation is written as the integral over all frequencies of the spectral radiative flux so the energy equation is[10]

$$k\frac{d^2T}{dx^2} - \frac{d}{dx}\int_0^\infty dq_{\nu r} = 0 \qquad (1)$$

Equation (1) will be integrated twice to obtain an expression for the temperature distribution within the medium. The integrations introduce two constants of integration that are eliminated by use of boundary conditions.

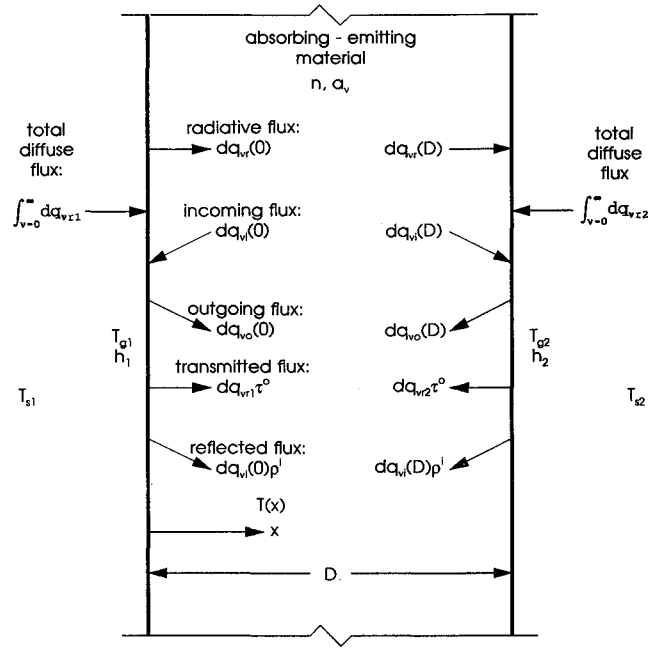

Fig. 1 Layer geometry, coordinate system, and nomenclature for radiative fluxes.

Equation (1) is integrated once and equated to its value at either $x = 0$ or $x = D$ to give

$$k\left.\frac{dT}{dx}\right|_x - \int_0^\infty dq_{\nu r}(x) = \text{constant}$$
$$= k\left.\frac{dT}{dx}\right|_0 - \int_0^\infty dq_{\nu r}(0) = k\left.\frac{dT}{dx}\right|_D - \int_0^\infty dq_{\nu r}(D) \qquad (2)$$

There are two types of imposed external conditions: convection from gases on both sides of the layer, and diffuse radiation incident from the surroundings on each side. After suitably accounting for boundary reflections, radiation passes into the layer and interacts within the material volume. There is no absorption at the interface because it does not have any volume. Hence, the conduction derivative terms at the boundaries in Eq. (2) are equated to only the convection to yield

$$-k\left.\frac{dT}{dx}\right|_x + \int_0^\infty dq_{\nu r}(x) = h_1[T_{g1} - T(0)] + \int_0^\infty dq_{\nu r}(0)$$
$$= h_2[T(D) - T_{g2}] + \int_0^\infty dq_{\nu r}(D) \qquad (3)$$

The energy equation in the form of Eq. (3) is now integrated a second time to yield an expression for the layer temperature distribution. The value of $T(0)$ is used for the constant of integration; the unknown $T(0)$ will be evaluated as part of the solution. The integration yields an expression for $T(x)$

$$T(x) = T(0) - \frac{h_1}{k}[T_{g1} - T(0)]x - \frac{x}{k}\int_0^\infty dq_{\nu r}(0)$$
$$+ \frac{1}{k}\int_0^x \left[\int_0^\infty dq_{\nu r}(x)\right] dx \qquad (4)$$

Evaluating Eq. (4) at $x = D$ yields an expression for the temperature difference across the layer as

$$T(D) - T(0) = -\frac{h_1}{k}[T_{g1} - T(0)]D - \frac{D}{k}\int_0^\infty dq_{\nu r}(0)$$
$$+ \frac{1}{k}\int_0^D \left[\int_0^\infty dq_{\nu r}(x)\right] dx \qquad (5)$$

This temperature difference is written in the form $[T(D) - T_{g2}] + [T_{g1} - T(0)] + (T_{g2} - T_{g1})$. The values in the square brackets are now replaced by their values obtained from Eq. (3) to yield

$$T(D) - T(0) = \frac{h_1}{h_2}[T_{g1} - T(0)] + \frac{1}{h_2}\int_0^\infty dq_{\nu r}(0) - \frac{1}{h_2}\int_0^\infty dq_{\nu r}(D) + [T_{g1} - T(0)] + (T_{g2} - T_{g1}) \quad (6)$$

This is equated to Eq. (5) and the result solved to yield an expression for $T(0)$ as

$$T(0) = T_{g1} + \left[\frac{h_1}{h_2} + 1 + \frac{h_1 D}{k}\right]^{-1} \times \left\{\int_0^\infty dq_{\nu r}(0)\left[\frac{1}{h_2} + \frac{D}{k}\right] - \frac{1}{h_2}\int_0^\infty dq_{\nu r}(D) + (T_{g2} - T_{g1}) - \frac{1}{k}\int_0^D\left[\int_0^\infty dq_{\nu r}(x)\right]dx\right\} \quad (7)$$

Relations for Radiative Flux

Equations (4) and (7) for the temperature distribution contain the spectral radiative flux $dq_{\nu r}(x)$, so this is now considered. The final set of equations will provide a coupled set of relations between the temperature distribution and the spectral radiative flux distribution. For a plane layer, the spectral radiative flux in the interval $d\nu$ is given by[10]

$$dq_{\nu r}(x) = 2\,dq_{\nu o}(0)E_3(a_\nu x) - 2\,dq_{\nu o}(D)E_3[a_\nu(D - x)] + 2n^2\left\{\int_0^x a_\nu e_{\nu b}(x^*)\,d\nu E_2[a_\nu(x - x^*)]\,dx^* - \int_x^D a_\nu e_{\nu b}(x^*)\,d\nu E_2[a_\nu(x^* - x)]\,dx^*\right\} \quad (8)$$

where $e_{\nu b}$ is used here for $n = 1$ in order to explicitly show the n^2 factor for internal emission. Equation (8) gives the spectral radiative flux at x inside the layer, and has in it terms for the diffuse spectral fluxes $dq_{\nu o}(0)$ and $dq_{\nu o}(D)$ that leave the *internal* surface of each boundary and propagate into the medium (see Fig. 1). These fluxes must be expressed in terms of the fluxes incident from the outside of the region to provide coupling with the radiative conditions imposed by the outside environment.

At the diffuse interfaces the spectral fluxes are related to the transmission of external flux and the reflection of internal flux by (Fig. 1):

$$dq_{\nu o}(0) = dq_{\nu r1}\tau_\nu^o + dq_{\nu i}(0)\rho_\nu^i \quad (9a)$$

$$dq_{\nu o}(D) = dq_{\nu r2}\tau_\nu^o + dq_{\nu i}(D)\rho_\nu^i \quad (9b)$$

Also on the inside of the two boundaries there are the following relations between the radiative flux and the outgoing and incoming fluxes (Fig. 1):

$$dq_{\nu r}(0) = dq_{\nu o}(0) - dq_{\nu i}(0) \quad (10a)$$

$$dq_{\nu r}(D) = -dq_{\nu o}(D) + dq_{\nu i}(D) \quad (10b)$$

By evaluating Eq. (8) at $x = 0$ and at $x = D$ and comparing with Eqs. (10a) and (10b), it is evident that the incoming fluxes are

$$dq_{\nu i}(0) = 2\,dq_{\nu o}(D)E_3(a_\nu D) + 2n^2\int_0^D a_\nu e_{\nu b}(x^*)\,d\nu E_2(a_\nu x^*)\,dx^* \quad (11a)$$

$$dq_{\nu i}(D) = 2\,dq_{\nu o}(0)E_3(a_\nu D) + 2n^2\int_0^D a_\nu e_{\nu b}(x^*)\,d\nu E_2[a_\nu(D - x^*)]\,dx^* \quad (11b)$$

The $dq_{\nu i}(0)$ are now eliminated between Eqs. (9) and (11), and the resulting equations placed into the form

$$dq_{\nu o}(0) - A_\nu\,dq_{\nu o}(D) = C_{\nu 1} \quad (12a)$$

$$dq_{\nu o}(D) - A_\nu\,dq_{\nu o}(0) = C_{\nu 2} \quad (12b)$$

where

$$A_\nu \equiv 2\rho_\nu^i E_3(a_\nu D) \quad (12c)$$

$$C_{\nu 1} \equiv \tau_\nu^o\,dq_{\nu r1} + 2n^2\rho_\nu^i\int_0^D a_\nu e_{\nu b}(x^*)\,d\nu E_2(a_\nu x^*)\,dx^* \quad (12d)$$

$$C_{\nu 2} \equiv \tau_\nu^o\,dq_{\nu r2} + 2n^2\rho_\nu^i\int_0^D a_\nu e_{\nu b}(x^*)\,d\nu \times E_2[a_\nu(D - x^*)]\,dx^* \quad (12e)$$

The two simultaneous Eqs. (12a) and (12b) are solved for $dq_{\nu o}(0)$ and $dq_{\nu o}(D)$ to yield

$$dq_{\nu o}(0) = \frac{C_{\nu 1} + A_\nu C_{\nu 2}}{1 - A_\nu^2} \quad (13a)$$

$$dq_{\nu o}(D) = \frac{C_{\nu 2} + A_\nu C_{\nu 1}}{1 - A_\nu^2} \quad (13b)$$

The solution can now be obtained by iteration as will be described. Then a banded model will be formulated and the equations placed in dimensionless form for calculating results.

Solution Procedure

An iterative solution is obtained by assuming a temperature distribution within the layer as the first step. To resolve the spectral dependence, a sufficient number of frequency values are selected to provide the desired accuracy when a numerical integration is carried out over frequency to obtain the total energy. The A_ν, $C_{\nu 1}$, and $C_{\nu 2}$ are evaluated from Eq. (12) at each ν and are used to calculate $dq_{\nu o}$ from Eq. (13). The $dq_{\nu r}(x)$ is then obtained from Eq. (8). The $T(0)$ is evaluated from Eq. (7), and $T(x)$ obtained from Eq. (4). This temperature distribution is used to begin the iteration again, and the process continued until a converged solution is obtained. Results for $n = 1$ were checked against those in Ref. 6 and the agreement was excellent. The solution procedure is now given more specifically for a banded situation.

Relations for Banded Model

For a banded formulation, the absorption coefficient has a constant value in each designated spectral region. The a_k applies in the kth frequency band extending from ν_k to ν_{k+1}. If the τ_ν^o and ρ_ν^i vary with frequency they must also be constant within the band. The integration of Eq. (12a) over the kth band yields, for example:

$$\Delta q_{ko}(0) - A_k\Delta q_{ko}(D) = C_{k1} \quad (14a)$$

where

$$A_k = 2\rho_k^i E_3(a_k D) \tag{14b}$$

$$C_{k1} = \tau_k^o \Delta q_{kr1} + 2n^2\rho_k^i \int_0^D a_k \sigma T^4(x^*) F_k(T) E_2(a_k x^*)\, dx^* \tag{14c}$$

and similarly for C_{k2}. The $F_k(T)$ is the fraction of energy in the kth frequency band for a blackbody at temperature $T(x^*)$. Using the A_k, C_{k1}, and C_{k2}, Eqs. (13) are used to obtain $\Delta q_{ko}(0)$ and $\Delta q_{ko}(D)$ for each band. Then from Eq. (8) the radiative flux at x in the kth band is obtained from

$$\Delta q_{kr}(x) = 2\Delta q_{ko}(0) E_3(a_k x) - 2\Delta q_{ko}(D) E_3[a_k(D - x)] + 2n^2 \left[\int_0^x a_k \sigma T^4(x^*) F_k(T) E_2[a_k(x - x^*)]\, dx^* - \int_x^D a_k \sigma T^4(x^*) F_k(T) E_2[a_k(x^* - x)]\, dx^* \right] \tag{15}$$

The three integrations over all frequencies that are in Eq. (7) are then carried out by summing over the bands

$$q_r(x) = \int_0^\infty dq_{\nu r}(x) = \sum_k \Delta q_{kr}(x) \tag{16}$$

Eqs. (7) and (6) become

$$T(0) = T_{g1} + \left[\frac{h_1}{h_2} + 1 + \frac{h_1 D}{k} \right]^{-1} \left\{ q_r(0) \left[\frac{1}{h_2} + \frac{D}{k} \right] - \frac{1}{h_2} q_r(D) + (T_{g2} - T_{g1}) - \frac{1}{k} \int_0^D q_r(x)\, dx \right\} \tag{17}$$

$$T(D) - T(0) = \frac{h_1}{h_2} [T_{g1} - T(0)] + \frac{1}{h_2} q_r(0) - \frac{1}{h_2} q_r(D) + [T_{g1} - T(0)] + (T_{g2} - T_{g1}) \tag{18}$$

Equations in Dimensionless Form

Using the dimensionless groups defined in the *Nomenclature*, the equations needed for the iterative solution have the dimensionless forms

Boundary Relations

$$A_k = 2\rho_k^i E_3(\kappa_{Dk}) \tag{19a}$$

$$\tilde{C}_{k1} = \tau_k^o \Delta \tilde{q}_{kr1} + 2n^2 \rho_k^i \kappa_{Dk} \int_0^1 t^4(X) F_k(T) \times E_2(\kappa_{Dk} X)\, dX \tag{19b}$$

$$\tilde{C}_{k2} = \tau_k^o \Delta \tilde{q}_{kr2} + 2n^2 \rho_k^i \kappa_{Dk} \int_0^1 t^4(X) F_k(T) \times E_2[\kappa_{Dk}(1 - X)]\, dX \tag{19c}$$

$$\Delta \tilde{q}_{\nu o}(0) = \frac{\tilde{C}_{\nu 1} + A_\nu \tilde{C}_{\nu 2}}{1 - A_\nu^2} \tag{20a}$$

$$\Delta \tilde{q}_{\nu o}(1) = \frac{\tilde{C}_{\nu 2} + A_\nu \tilde{C}_{\nu 1}}{1 - A_\nu^2} \tag{20b}$$

Flux Relations

$$\Delta \tilde{q}_{kr}(X) = 2\Delta \tilde{q}_{ko}(0) E_3(\kappa_{kD} X) - 2\Delta \tilde{q}_{ko}(1) E_3[\kappa_{kD}(1 - X)] + 2n^2 \kappa_{kD} \left[\int_0^X t^4(X^*) F_k(T) E_2[\kappa_{kD}(X - X^*)]\, dX^* - \int_X^1 t^4(X^*) F_k(T) E_2[\kappa_{kD}(X^* - X)]\, dX^* \right] \tag{21}$$

$$\tilde{q}_r(X) = \sum_k \Delta \tilde{q}_{kr}(X) \tag{22}$$

Temperature Relations

$$t(0) = 1 + \left[R + 1 + \frac{H_R}{N_D} \right]^{-1} \left\{ t_{g2} - 1 + \frac{1}{H_R} \times \left[\left(R + \frac{H_R}{N_D} \right) \tilde{q}_r(0) - R\tilde{q}_r(1) - \frac{H_R}{N_D} \int_0^1 \tilde{q}_r(X)\, dX \right] \right\} \tag{23}$$

$$t(X) = t(0) - \frac{1}{N_D} \left\{ H_R[1 - t(0)]X - \tilde{q}_r(0)X + \int_0^X \tilde{q}_r(X)\, dX \right\} \tag{24}$$

Relations for Diffuse Interface Transmittance and Reflectance

For diffuse interfaces the roughness will influence τ^o, which is for radiation incident from the outside, and ρ^i, which is for radiation incident from inside the layer. When the refractive index of the medium is greater than unity, ρ^i must include the effect that some of the internal radiation is totally reflected by the interface. In the absence of other information, the diffuse interface characteristics for small roughness were determined by integrated averages from the Fresnel reflection relations.

The externally incident radiation is diffuse. By integrating the reflected energy over all incident angles the relation for τ^o is given by[11]

$$\tau^o(n) = 1 - \rho^o(n) = \frac{1}{2} - \frac{(3n + 1)(n - 1)}{6(n + 1)^2} - \frac{n^2(n^2 - 1)^2}{(n^2 + 1)^3} \mathcal{K}\left(\frac{n - 1}{n + 1} \right) + \frac{2n^3(n^2 + 2n - 1)}{(n^2 + 1)(n^4 - 1)} - \frac{8n^4(n^4 + 1)}{(n^2 + 1)(n^4 - 1)^2} \mathcal{K}(n) \tag{25}$$

This assumes the interface properties can be calculated by considering the medium to be a perfect dielectric; that is, the effect of the extinction coefficient in the complex index of refraction can be neglected. This is a good assumption unless the extinction coefficient is large.[12,13] Hence, the interface properties used here are a function of only the simple index of refraction n. After allowance for energy that is at angles larger than the critical angle for total reflection, the ρ^i is found as a function of n from[11]

$$\rho^i(n) = 1 - \frac{\tau^o(n)}{n^2} \tag{26}$$

Values of τ^o and ρ^i are in Table 1 for various n. It is evident that as n increases, there is substantial internal reflection.

Table 1 Interface properties

n	External τ^o	Internal ρ^i
1.0	1.0	0
1.5	0.90822	0.59635
2.0	0.83940	0.79015
2.5	0.77813	0.87550
3.0	0.72380	0.91958
3.5	0.67579	0.94483
4.0	0.63336	0.96041
4.5	0.59573	0.97058
5.0	0.56222	0.97751

Numerical Solution Method

The numerical solution of Eq. (21) requires integrating the fourth power of the temperature distribution multiplied by the exponential integral function E_2. Because E_2 is well behaved, the integrals were evaluated without difficulty using the Gaussian integration subroutine QDAGS from the IMSL library. The layer was divided into evenly spaced grid points; by trying various grid sizes, 41 points were found to be sufficient. The $t^4(X)$ distribution was fitted during each iteration by the cubic spline subroutine CSINT. The Gaussian subroutine called for unevenly spaced grid points, and, as required during the calculations, they were interpolated from the spline fit.

The blackbody fraction F_k was evaluated as required during the solution by use of the rapidly converging series[14]

$$F_k(T) = F_{0-\nu_{k,b}}(T) - F_{0-\nu_{k,a}}(T) \tag{27a}$$

where

$$F_{0-\nu}(T) = 1 - \frac{15}{\pi^4}\sum_m \frac{e^{-m\beta}}{m}\left(\beta^3 + \frac{3\beta^2}{m} + \frac{6\beta}{m^2} + \frac{6}{m^3}\right) \tag{27b}$$

and $\beta = C_2\nu/c_0T$.

Special Cases for Transparent and Opaque Layers

Transparent Layer

For a transparent layer, there is no radiative interaction with the layer. The boundaries are heated or cooled by convection, and internal heat flow is by conduction. Using ordinary relations for heat flow through a plane layer yields in dimensionless form

$$t(0) = 1 - \frac{1 - t_{g2}}{1 + \dfrac{H_R}{N_D} + R} \tag{28a}$$

$$t(1) = t(0) - \frac{H_R}{N_D}[1 - t(0)] \tag{28b}$$

Opaque Layer

For an opaque layer, there are additional terms for absorption and emission at the boundaries. The boundary emissivities are independent of frequency for the present analysis. The solution is obtained from the following three equations; Eqs. (29a) and (29c) are from a heat balance at each of the interfaces, and Eq. (29b) is the relation for heat conduction through the layer

$$H_R[1 - t(0)] + \varepsilon_1[1 - t^4(0)] - \tilde{q} = 0 \tag{29a}$$

$$N_D[t(0) - t(1)] - \tilde{q} = 0 \tag{29b}$$

$$\frac{H_R}{R}[t(1) - t_{g2}] + \varepsilon_2[t^4(1) - t_{g2}^4] - \tilde{q} = 0 \tag{29c}$$

For opaque gray surfaces, ε_1 and ε_2 depend on n and are both equal to $1 - \rho^o = \tau^o$ obtained from Eq. (25).

Results and Discussion

Results are given first for a gray layer. As shown, this provides a framework for explaining the two-band solutions that follow.

Temperature Distributions and Surface Temperatures for a Gray Layer

The analysis is formulated in a general way with unequal amounts of radiative heating imposed at the two sides of the semitransparent layer. The radiative heating is specified independently of the gas temperature on each side that provides the convective heat transfer. To reduce somewhat the number of parameters and still provide insight into the physical behavior, the following conditions were selected for the results given here. The environment on each side of the layer is black and has a temperature equal to the gas temperature on that side. The incident radiant fluxes, then are, $q_{r1} = \sigma T_{g1}^4$ and $q_{r2} = \sigma T_{g2}^4$. The gas temperature on the cold side (side 2 in Fig. 1) is one-quarter that on the hot side (side 1). When the ratio of gas temperatures was changed to one-half, similar results were obtained and are not included here. The convective heat transfer coefficients on the two sides are equal to each other, so the parameter $R = 1$. The convection-to-radiation parameter H_R is varied from 0.1 to 10, that corresponds, for example, to heat transfer coefficients from 19.14 to 1914 W/m²·K when $T_{g1} = 1500$ K. The conduction-radiation parameter N_D is varied from 0.1 to 10, corresponding, for example, to thermal conductivities from 0.19 to 19.14 W/m·K for a layer 1 cm thick with $T_{g1} = 1500$ K.

Effect of Index of Refraction

For the first set of results (Fig. 2), convection is of the same order as the external radiation provided to the hot side, so $H_R = 1.0$. The conduction parameter is rather small, $N_D = 0.1$; this provides a significant influence of internal radiation on the temperature distribution rather than it being dominated by heat conduction. The three parts of the figure are for indexes of refraction, $n = 1$, 2, and 4. Each part provides temperature distributions within the layer for optical thicknesses κ_D covering the range 0 to ∞. For small and large optical thicknesses, the results approach the limiting cases for transparent and opaque layers computed from the special cases, Eqs. (28) and (29). The comparisons were found to be excellent as κ_D in the general computer program was made very small or very large.

The limiting cases provide linear temperature distributions because energy transport within the material is only by conduction. For the parameters in Fig. 2, the limiting cases yield temperature distributions that are close to each other. This shows that, for these parameters, the surface radiation absorption and emission in the opaque case (absent for the transparent case) are not very significant relative to the convective heating. In contrast, when κ_D is neither very small nor very large, there is a substantial internal radiation effect. For intermediate κ_D, radiation penetrates into the interior of the layer and internal exchange occurs. The result in Fig. 2a (for $n = 1$) is that as the optical thickness is increased from zero to approximately 1, the temperature profiles become less linear, and the temperatures increase. The temperatures then decrease as κ_D is further increased (except at small X), and become more linear as the layer becomes optically thick. As $\kappa_D \to \infty$, the opaque limit is reached, which, for the present conditions, happens to be close to the transparent limit.

Consider now the effect of increasing the index of refraction; results for $n = 2$ and 4 are in Figs. 2b and 2c. Because internal volume emission is proportional to n^2, this produces a considerable increase in internal emission. There is also a substantial increase in total reflection at the internal boundaries (see Table 1) because the radiation flux leaving the layer cannot exceed that of a blackbody. The internal reflections

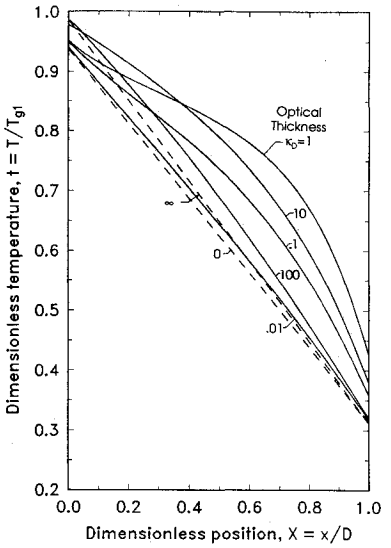

a) $n = 1$

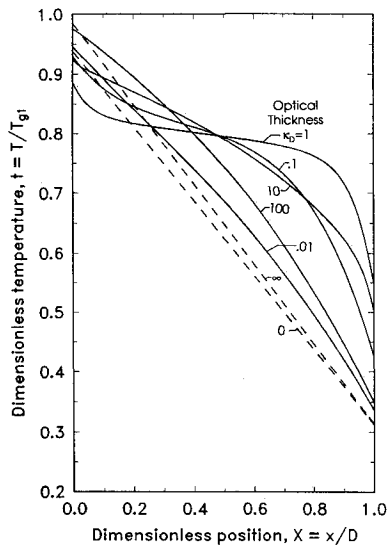

b) $n = 2$

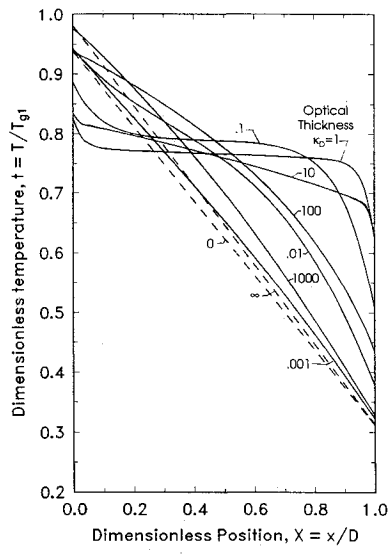

c) $n = 4$

Fig. 2 Effect of index of refraction on temperature distributions; $t_{s1} = t_{g1} = 1.0$, $t_{s2} = t_{g2} = 0.25$, $N_D = 0.1$, and $H_R = 1.0$.

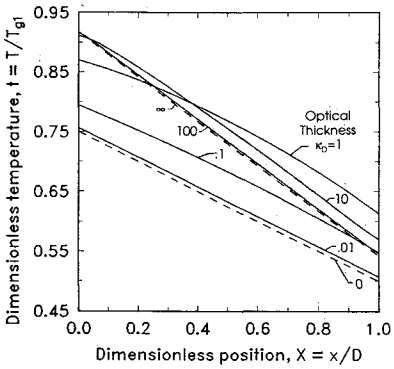

a) $n = 1$

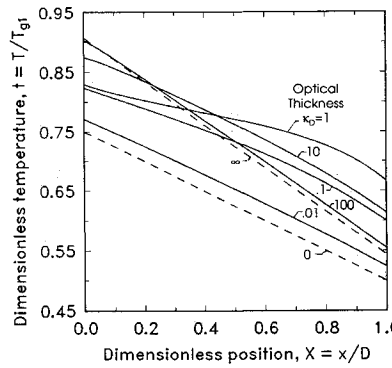

b) $n = 2$

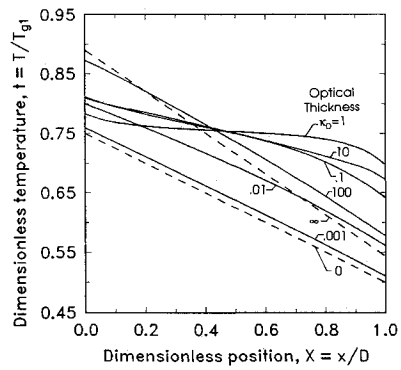

c) $n = 4$

Fig. 3 Effect of index of refraction and increased thermal conductivity on temperature distributions; $t_{s1} = t_{g1} = 1.0$, $t_{s2} = t_{g2} = 0.25$, $N_D = 1.0$, and $H_R = 1.0$.

produce a substantial radiative exchange across the layer that tends to equalize the temperature distribution. As shown in Fig. 2c for $n = 4$, this effect is strong for intermediate values of the optical thickness $\kappa_D = 0.1$–10. For very small or large κ_D, this effect decreases, and the limiting cases with linear temperature distributions are approached.

The effect on the internal temperature distributions of increasing the heat conduction is in Fig. 3. This shows how the distributions in Fig. 2 change when N_D is increased from 0.1 to 1.0. This has the expected effect of reducing the temperature variations within the layer. Because the relative effect of radiation is reduced, the profiles are more linear in shape. The relative positions of some of the curves are also changed. Another effect is that the limiting profiles for $\kappa_D \to 0$ and ∞ are separated more than for the conditions in Fig. 2.

Effect of Convection at Interfaces

The results in Figs. 2 and 3 are for an intermediate value of the convection parameter H_R. Figure 4 shows the effect of having smaller and larger amounts of convection. The results are for $\kappa_D = 1.0$, that was found in Figs. 2 and 3 to be in the range that provides the largest radiative effect on the tem-

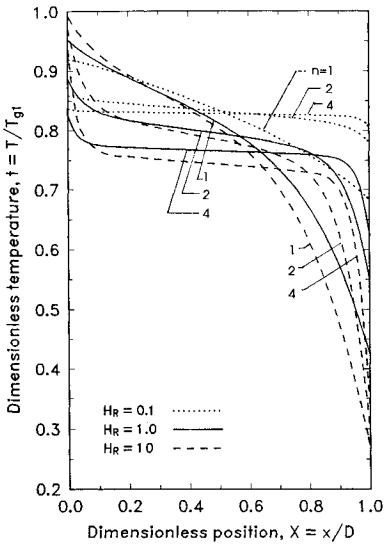

Fig. 4 Effect of index of refraction and convection at interfaces on temperature distributions; $t_{s1} = t_{g1} = 1.0$, $t_{s2} = t_{g2} = 0.25$, $N_D = 0.1$, and $\kappa_D = 1.0$.

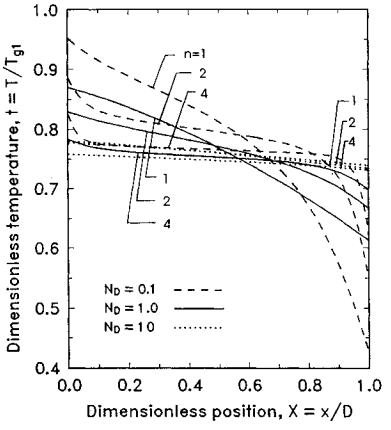

Fig. 5 Effect of index of refraction and heat conduction on temperature distributions; $t_{s1} = t_{g1} = 1.0$, $t_{s2} = t_{g2} = 0.25$, $H_R = 1.0$, and $\kappa_D = 1.0$.

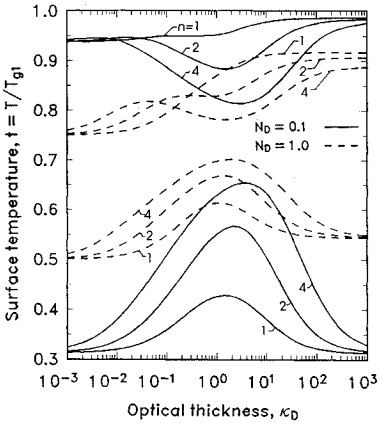

Fig. 6 Effect of optical thickness, index of refraction, and heat conduction on layer surface temperatures; $t_{s1} = t_{g1} = 1.0$, $t_{s2} = t_{g2} = 0.25$, and $H_R = 1.0$.

perature distributions. A large H_R tends to move the surface temperatures toward the gas temperatures. For small convection, the profiles become rather flat. There is a very substantial effect of the index of refraction. As n increases, the temperature profiles become more uniform in the central region of the layer. For $n = 4$, there is only a very small temperature variation in the central region. This coupled with large convection effects when $H_R = 10$, produces large internal temperature gradients near the boundaries.

Effect of Internal Heat Conduction

The effect of the parameter N_D is examined in Fig. 5. Increasing N_D corresponds to increased internal heat conduction. When $N_D = 10$, internal conduction is so large that the temperature is practically constant across the layer. In contrast, for $N_D = 0.1$, there are substantial gradients within the layer. These become large adjacent to the boundaries when the index of refraction is increased because a large n tends to equalize the temperatures within the central portion of the layer by means of internal reflections. As shown in Fig. 4, the gradients are considerably increased as surface convection is raised.

Surface Temperatures of Layer

To show in more detail some aspects of the effects of optical thickness and index of refraction on the layer temperatures, the surface temperatures are examined. Results are in Fig. 6 for $N_D = 0.1$ and 1.0. For $N_D = 0.1$, the transparent and opaque limiting cases happen to yield surface temperatures that are almost equal. Hence, as the optical thickness is increased from zero, each surface temperature varies through a maximum or minimum value, except at the higher temperature side when $n = 1$, where the surface temperature increases slightly with κ_D. The maximum and minimum values occur for κ_D between 1 and 5. Although a large n tends to equalize the temperatures within the interior of the layer, it produces the largest surface temperature variations with κ_D. There is little effect of n on the surface temperatures when κ_D is either very small or very large. When N_D is increased to 1.0, the shape of the upper set of curves is changed from that for $N_D = 0.1$. Now the minimum temperature occurs at the smallest κ_D, and the temperatures at the hotter side vary between those for the limiting cases of $\kappa_D \to 0$ and ∞.

Apparent Surface Temperature Calculated from Radiative Energy Leaving Interface

When making radiation measurements to determine temperatures of semitransparent layers, the radiant energy leaving the layer is detected and converted to an indicated surface temperature. The radiant energy leaving the surface consists of emitted, transmitted, and reflected energy. It is assumed here that a correction is made to remove the effect of the energy reflected from the outside of the observed surface. In Fig. 7, the apparent surface temperature t_a, computed using the diffuse energy flux leaving each side of the layer, is compared to the actual calculated surface temperatures as given in Fig. 6. The energy used to determine the apparent surface temperature is that emitted by the layer combined with energy transmitted through the layer from that supplied to the other side. The diffuse surface emissivity is equal to $1 - \rho^o = \tau^o$

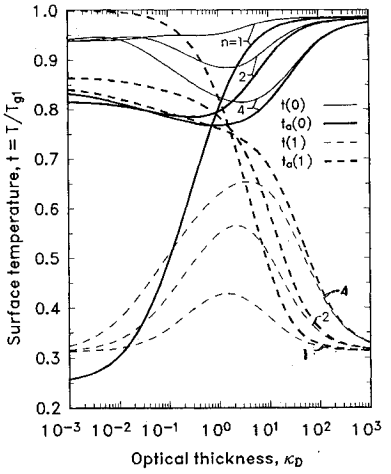

Fig. 7 Effect of optical thickness and index of refraction on apparent surface temperature computed from radiative flux; $t_{s1} = t_{g1} = 1.0$, $t_{s2} = t_{g2} = 0.25$, $N_D = 0.1$, and $H_R = 1.0$.

as obtained from Eq. (25). Then, in dimensionless form, the apparent temperature at each surface is $t_a = [\tilde{q}_i(1 - \rho^i)/\tau^o]^{1/4}$. Figure 7 gives results when the conduction parameter is $N_D = 0.1$. Using $N_D = 1.0$ gave similar behavior so the results are not included here. The curves give the apparent surface temperatures for the hot and cold sides for refractive indexes $n = 1$, 2, and 4.

First consider the results for the cold side. For very small optical thicknesses, the layer does not emit or absorb significant radiation, but for $n > 1$, there are reflection effects at the interfaces. Radiant energy from the surroundings on the hot side is transmitted through the layer and yields a high apparent surface temperature at the cold side. When n is increased to 2 or 4, there is a decrease in the transmitted energy. This is partly due to reflection from the outside of the hot side interface. The energy that passes into the layer is diffused by the rough interface, so part of it is totally reflected when it reaches the inside of the interface at the cold side. The multiple reflections prevent a portion of the energy from being transmitted, thus lowering the apparent surface temperature. As the optical thickness is increased, the layer begins to absorb incident energy internally and internal reemission occurs. For large κ_D, the transmitted energy is blocked by the rather opaque layer. The energy leaving is then primarily by emission. For optical thicknesses greater than approximately 30, the energy leaving through the interface yields fairly accurate surface temperature predictions. For a conduction parameter $N_D = 1.0$, approximately the same predictive accuracy is obtained when $\kappa_D = 10$.

For the hot side, when $n = 1$ and the optical thickness is very small, the energy leaving the colder surroundings is transmitted and yields a low apparent surface temperature. For $n = 2$ and 4 and very small optical thicknesses, a significant portion of the energy passing into the layer from the hot side is totally reflected when it reaches the inside of the interface at the cold side. The subsequent multiple reflections significantly increase the apparent surface temperature at the hot side. For large κ_D, energy transmission is being blocked and the effects of multiple internal reflections are thereby decreased. Energy is leaving primarily by emission. For optical thicknesses greater than approximately 10, fairly accurate hot side surface temperature measurements can be made for $N_D = 0.1$ and 1.0.

Nongray Effects on Temperature Distributions

The previous results have been for a gray layer; they are now shown to provide considerable insight into the behavior of a nongray layer. Some results are given here for a two-band model where the layer optical thickness changes in a step fashion from a small to a larger value as wavelength is increased (frequency is decreased). Although frequency (that does not change with n when crossing an interface) has been used as the convenient spectral variable in the analysis, the cutoff location is given here in terms of wavelength, that is common in the literature. Because the incident energy is from a medium with $n = 1$, the parameter $\lambda_c T_{g1}$ determines the fractional amount of energy from a blackbody source at T_{g1} that is on either side of the cutoff λ_c. Additional parameters are the individual values of κ_D on either side of λ_c; these are κ_s and κ_l for the short and long wavelength regions. When $\lambda_c T_{g1}$ is small, the fraction of blackbody radiation in the short wavelength region is very small, so the layer has an optical thickness $\kappa_D \approx \kappa_l$. When $\lambda_c T_{g1}$ is large, the fraction of blackbody radiation in the short wavelength region is large and the layer has an optical thickness $\kappa_D \approx \kappa_s$.

Temperature distributions for three $\lambda_c T_{g1}$ are in Fig. 8 for the same parameters as Fig. 3b ($n = 2$) and with $\kappa_s = 1$ and $\kappa_l = 10$. The temperature distributions occupy a narrow range. They are between the limiting curves for gray layers with $\kappa_D = 1$ and 10 in Fig. 3(b) that correspond to when $\lambda_c T_{g1} \to \infty$ and 0. Thus, the gray results provide considerable insight for the temperature distributions in a two-band spectral layer.

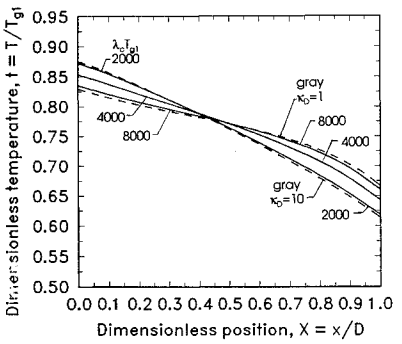

Fig. 8 Nongray effects on temperature distributions, $t_{s1} = t_{g1} = 1.0$, $t_{s2} = t_{g2} = 0.25$, $H_R = 1.0$, $n = 2$, $\kappa_s = 1.0$, $\kappa_l = 10$, and $N_D = 1.0$.

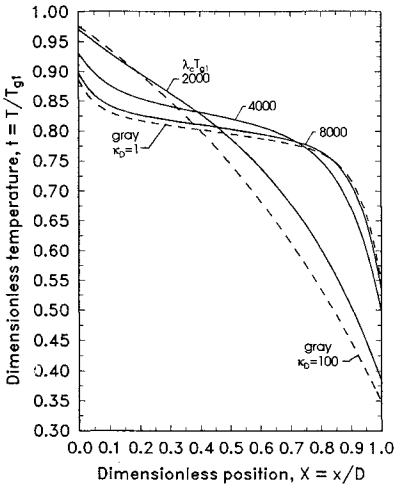

Fig. 9 Nongray effects on temperature distributions, $t_{s1} = t_{g1} = 1.0$, $t_{s2} = t_{g2} = 0.25$, $H_R = 1.0$, $n = 2$, $\kappa_s = 1.0$, $\kappa_l = 100$, and $N_D = 0.1$.

This is shown in Fig. 9 for another set of nongray results. These are for the same parameters ($n = 2$) as in Fig. 2b and for $\kappa_s = 1$ and $\kappa_l = 100$. The limiting cases for large and small $\lambda_c T_{g1}$ correspond to the gray cases for $\kappa_D = 1$ and 100 that are shown to be somewhat apart in Fig. 2b. The nongray results for various $\lambda_c T_{g1}$ in Fig. 9 stay within, or close to, the envelope of the gray curves. The temperature profile for the lowest $\lambda_c T_{g1}$ is similar to the $\kappa_D = 100$ gray case, while the profiles for $\lambda_c T_{g1} \geq 4000$ are similar to the $\kappa_D = 1$ gray case.

Conclusions

Temperature distributions and other heat transfer characteristics have been examined for a semitransparent plane layer subjected to heating on both sides by convection and radiation. The layer has diffuse interfaces and a refractive index ≥ 1. This simulates, for example, a frosted window used to diffuse incident radiation in a high-temperature experiment, or a ceramic material with small scattering in high-temperature applications. An index of refraction larger than unity has a substantial effect on the temperature distributions. This is caused by the large amount of internal energy reflection that tends to make the temperature distributions more uniform within the layer. Near the boundaries there can be large effects resulting from external convection. The combined internal and interface effects tend to produce large temperature gradients near the surfaces.

The analysis is formulated in a general way for a nongray material. Temperature distributions are first investigated in detail for a gray layer for the complete range of optical thickness from 0 to ∞. Then results are obtained for two-band nongray properties. For the nongray results, the optical thickness has a step-function change at a cutoff wavelength. Using the optical thicknesses on either side of the cutoff in the gray

solution, gives temperature profiles that are a very good guide to the bounds of the nongray solutions.

The energy leaving a layer surface by emission and by transmission from the other side, was examined to determine when it could be used to indicate the surface temperature for experimental measurements. It was found that for some conditions a layer optical thickness of 10 was sufficient to obtain a good surface temperature indication. For other parameters an optical thickness of 30 or larger was required.

References

[1]Gardon, R., "Calculation of Temperature Distributions in Glass Plates Undergoing Heat-Treatment," *Journal of the American Ceramic Society*, Vol. 41, No. 6, 1958, pp. 200–209.

[2]Fowle, A. A., Strong, P. F., Comstock, D. F., and Sox, C., "Computer Program to Predict Heat Transfer through Glass," *AIAA Journal*, Vol. 7, No. 3, 1969, pp. 478–483.

[3]Rokhsaz, F., and Dougherty, R. L., "Radiative Transfer Within a Finite Plane-Parallel Medium Exhibiting Fresnel Reflection at a Boundary," *Heat Transfer Phenomena in Radiation, Combustion and Fires*, ASME HTD-Vol. 106, 1989, pp. 1–8.

[4]Ping, T. H., and Lallemand, M., "Transient Radiative-Conductive Heat Transfer in Flat Glasses Submitted to Temperature, Flux and Mixed Boundary Conditions," *International Journal of Heat and Mass Transfer*, Vol. 32, No. 5, 1989, pp. 795–810.

[5]Crosbie, A. L., and Shieh, S. M., "Three-Dimensional Radiative Transfer for Anisotropic Scattering Medium with Refractive Index Greater Than Unity," *Journal of Quantitative Spectroscopy & Radiative Transfer*, Vol. 44, No. 2, 1990, pp. 299–312.

[6]Viskanta, R., and Grosh, R. J., "Heat Transfer by Simultaneous Conduction and Radiation in an Absorbing Medium," *Journal of Heat Transfer*, Vol. 84, No. 1, 1962, pp. 63–72.

[7]Amlin, D. W., and Korpela, S. A., "Influence of Thermal Radiation on the Temperature Distribution in a Semi-Transparent Solid," *Journal of Heat Transfer*, Vol. 101, No. 1, Feb. 1979, pp. 76–80.

[8]Tarshis, L. A., O'Hara, S., and Viskanta, R., "Heat Transfer by Simultaneous Conduction and Radiation for Two Absorbing Media in Intimate Contact," *International Journal of Heat and Mass Transfer*, Vol. 12, No. 3, 1969, pp. 333–347.

[9]Anderson, E. E., and Viskanta, R., "Spectral and Boundary Effects on Coupled Conduction-Radiation Heat Transfer Through Semitransparent Solids," *Wärme-und Stoffübertragung*, Vol. 6, No. 1, 1973, pp. 14–24.

[10]Siegel, R., and Howell, J. R., *Thermal Radiation Heat Transfer*, 2nd ed., Hemisphere, Washington, DC, 1981.

[11]Richmond, J. C., "Relation of Emittance to Other Optical Properties," *Journal of Research of the National Bureau of Standards*, Vol. 67C, No. 3, 1963, pp. 217–226.

[12]Cox, R. L., "Fundamentals of Thermal Radiation in Ceramic Materials," *Thermal Radiation in Solids*, edited by S. Katzoff, NASA SP-55, 1965, pp. 83–101.

[13]Hering, R. G., and Smith, T. F., "Surface Radiation Properties from Electromagnetic Theory," *International Journal of Heat and Mass Transfer*, Vol. 11, No. 10, 1968, pp. 1567–1571.

[14]*Planck's Radiation Functions and Electronic Functions*, A. N. Lowan, Technical Director, Federal Works Agency, Works Projects Admin., New York, under the sponsorship of U. S. National Bureau of Standards Computation Lab., 1941.